Eur. Phys. J. E **12**, 35–40 (2003)
DOI 10.1140/epje/i2003-10052-4

THE EUROPEAN PHYSICAL JOURNAL E

Molecular dynamics simulations of simple fluids confined in realistic models of nanoporous carbons

J. Pikunic and K.E. Gubbins[a]

Department of Chemical Engineering, North Carolina State University, 113 Riddick Labs, Raleigh, NC 27695-7905, USA

Received 1 January 2003 /
Published online: 30 October 2003 –

Abstract. We present molecular dynamics simulations in the micro-canonical ensemble of a Lennard-Jones model of nitrogen confined in realistic models for saccharose-based carbons developed in our previous work. We calculate the velocity autocorrelation function and mean-squared displacement, and the self-diffusivities from the latter. We observe that the self-diffusivity increases with temperature and exhibits a maximum with loading or adsorbate density. To the best of our knowledge, a maximum in self-diffusivities has not been observed in molecular dynamics simulations of fluids confined in slit pores.

PACS. 61.43.Gt Powders, porous materials – 68.43.Jk Diffusion of adsorbates, kinetics of coarsening and aggregation – 82.75.Fq Synthesis, structure determination, structure modeling

1 Introduction

In most molecular dynamics (MD) simulations of fluids in porous carbons, the adsorbent is modeled using the slit pore model, in which the pore volume is the space between two parallel and infinite graphite layers. In real carbons, however, the porous network is made up of inter-connected pores of different size and shape, and even different pore wall morphology [1]. Several models have been developed to include pore connectivity, differences in pore shape and size, and other sources of adsorbate-adsorbent energy heterogeneity. Some of these models are based on qualitative reconstructions of experimental structure data (*e.g.* transmission electron microscopy, and X-ray diffraction), while others attempt to include this information in quantitative ways. These models have been recently reviewed [1].

The first attempt to build a model for porous carbons that matches the structure factor or pair correlation function obtained from diffraction experiments was presented by Thomson and Gubbins [2]. They applied Reverse Monte Carlo (RMC) to develop a model composed of rigid and perfect graphene segments for an activated carbon. The RMC model of Thomson and Gubbins is reasonable for many graphitisable carbons with roughly aligned segments. However, the use of graphene segments, instead of individual carbon atoms, as the basic structural units fails to allow the formation of defects (*e.g.*, rings of 5 or 7 carbon atoms) that are important sources of heterogeneity of many porous carbons [1,3].

In a more recent work [3], we presented an atomistic approach in which carbon atoms, instead of graphene segments, undergo Monte Carlo moves that are accepted or rejected based on the agreement between the simulated and the experimental structure factor, $S(q)$. This procedure allows the formation of non-aromatic rings, small chains of carbon atoms, and other structures that are responsible for the curvature and cross-linking in graphene segments. We combined our atomistic approach with simulated annealing to develop a reconstruction method [4] that gives better fits to the experimental data than the original RMC technique. In our latest version [5,6], we use the Monte Carlo $g(r)$ method to obtain the pair correlation function, $g(r)$, from the experimental $S(q)$. We then use the resulting $g(r)$, instead of $S(q)$, as the target function in our reconstruction method. The two functions contain the same information and are related by a Fourier transformation. However, the calculation of $g(r)$ from the atomic positions is much faster than the calculation of $S(q)$. Therefore, this modification speeds up the simulations, allowing us to construct models in much larger simulation boxes (at least 5 times more volume).

We have used this reconstruction method to model two porous carbons produced by the pyrolysis of saccharose and subsequent heat treatment at two different temperatures (400 °C and 1000 °C) [6]. In this work, we report molecular dynamics simulations in the micro-canonical ensemble of a Lennard-Jones fluid confined in the two resulting models. We carried out the simulations at two different temperatures and four loadings. We calculated the velocity autocorrelation functions and mean-square displacements, and from these the self-diffusivities.

[a] e-mail: keg@ncsu.edu

2 Preparation of the model carbons

We used the two models of saccharose-based carbons developed in our previous work [6]. The carbons were prepared by pyrolysis of saccharose and subsequent heat treatment at two different temperatures: 400 °C (sample CS400) and 1000 °C (sample CS1000). X-ray diffraction and small-angle X-ray scattering (SAXS) experiments were performed to obtain the structure factor, $S(q)$, of both materials in the q-range 0.02–14.0 Å^{-1}. The Monte Carlo $g(r)$ (MCGR) [7,8] procedure was used to obtain the pair correlation function, $g(r)$. MCGR is an inverse procedure to obtain $g(r)$ from $S(q)$. In contrast with directly taking the inverse Fourier transform of the experimental $S(q)$, MCGR avoids the truncation errors caused by the limitations in the experimental data. The resulting $g(r)$ is shown in Figure 1. Our results for CS1000 are in excellent agreement with the pair correlation function calculated for the same material in an independent study [9] from X-ray diffraction data obtained for q-values up to 24 Å^{-1}, using synchrotron radiation.

We used the resulting $g(r)$ shown in Figure 1 as the target function in our reconstruction method. The details of our procedure are given in [6]. The idea is, as in the original RMC method [10], to obtain configurations that are consistent with the target $g(r)$ by minimizing the differences between the simulated and the target $g(r)$, quantified by the following parameter:

$$\chi^2 = \frac{\sum_{i=1}^{n_{\exp}} \left[g_{\mathrm{sim}}(r_i) - g_{\mathrm{target}}(r_i)\right]^2}{\sum_{i=1}^{n_{\exp}} \left[g_{\mathrm{target}}(r_i)\right]^2}, \qquad (1)$$

where $g_{\mathrm{sim}}(r_i)$ is the simulated $g(r)$ and $g_{\mathrm{target}}(r_i)$ is the target $g(r)$ evaluated at r_i. Naively matching the simulated $g(r)$ to the target $g(r)$, however, does not guarantee that the resulting configurations are unique or, moreover, that they have physical meaning. Some guidance concerning the uniqueness of the structures resulting from the RMC procedure is provided by the uniqueness theorem of statistical mechanics [11]. For systems in which the potential is pairwise additive, it can be shown that a given pair correlation function uniquely determines all the higher-order correlation functions [12,13]. The interatomic forces in a carbon material, however, do not correspond to pairwise potentials. There are angular contributions to the interaction potential that are, by definition, many-body interactions. When three-body forces are present, the uniqueness theorem of statistical mechanics states that for a given set of pair correlation function and three-body correlation function, all the higher-order correlation functions are uniquely determined. Thus, assuming that only two- and three-body forces are important, we use the pair correlation function along with a set of simple expressions to describe the three-body correlations to completely specify the structure of the system.

We assume that most carbon atoms are sp^2 hybridized. Following this assumption, the coordination number of each carbon is three. From composition data, we estimate the average carbon coordination number, and from this the target fraction of carbon atoms with three carbon

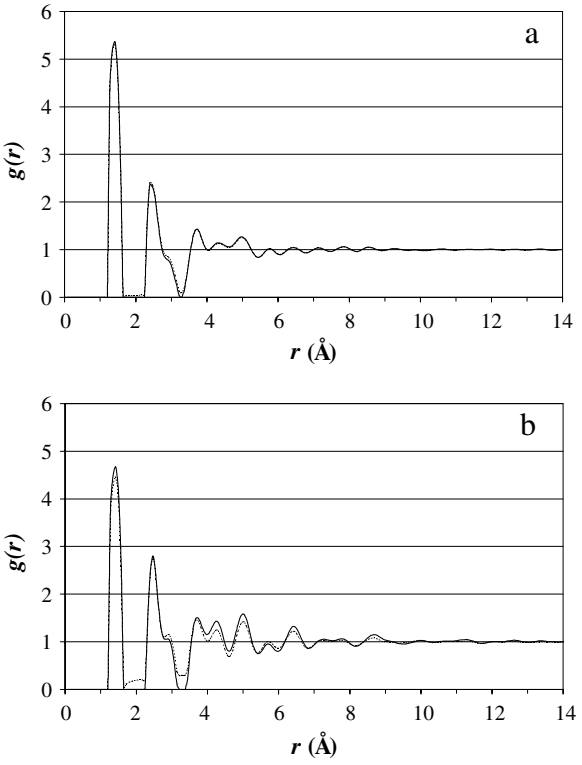

Fig. 1. Pair correlation functions of saccharose-based carbons obtained with MCGR (solid line) and reconstruction method (dashed line). a) CS400, b) CS1000. Taken from [6].

neighbors [6]. We can then use this quantity as the target to constrain the carbon coordination number in the model by minimizing the parameter

$$\delta^2 = \left[\left(\frac{N_3}{N}\right)_{\mathrm{sim}} - \left(\frac{N_3}{N}\right)_{\mathrm{target}}\right]^2, \qquad (2)$$

where N_3 is the number of carbon atoms with carbon coordination number of 3 and N is the total number of carbon atoms in the system. The simulated fraction of carbon atoms with carbon coordination number of 3 is easily calculated by counting how many carbon atoms in the simulation box have three neighbors at a distance between a minimum and a maximum bond length, equal to the distances at which the first peak in the pair correlation function begins and ends, respectively.

Also following the assumption of sp^2 hybridization, the equilibrium C-C-C angle distribution must be centered at 120°. The order parameter that describes the bond angle constraint is thus given by

$$\psi^2 = \frac{1}{n_\theta} \sum_{i=1}^{n_\theta} \left[\cos(\theta_i) - \cos\left(\frac{2\pi}{3}\right)\right]^2, \qquad (3)$$

where the θ_i's are the C-C-C bond angles in radians, and n_θ is the total number of bond angles. The use of the cosine function is consistent with the functional form of bond order potentials for carbon (*e.g.* Tersoff and Brenner potentials) [14–16].

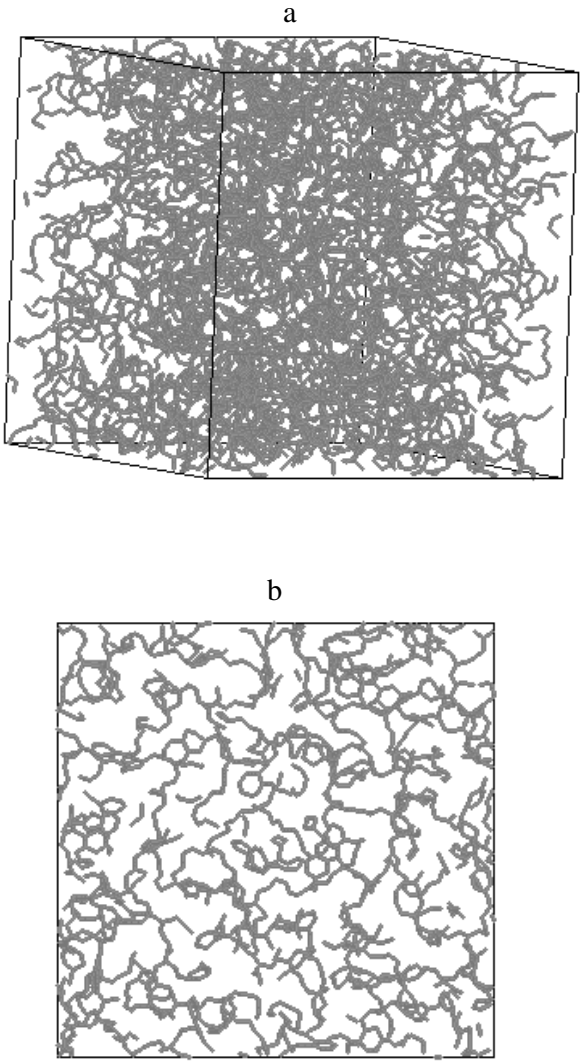

Fig. 2. Resulting structural model for CS400. (a) Snapshot of the 5 nm simulation box. (b) Projection of a 1.25 nm section of the simulation box. The gray rods represent C-C bonds.

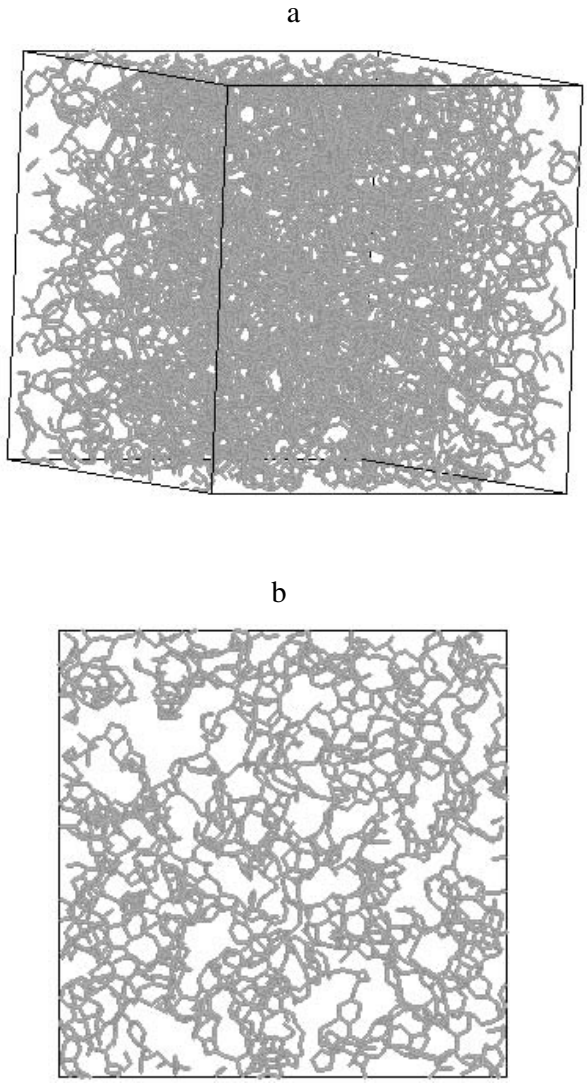

Fig. 3. As in Figure 2 for CS1000.

In our reconstruction procedure, we start from a random configuration of carbon atoms that has a density equal to that obtained from experiments. We then attempt Monte Carlo moves that consist of randomly selecting a carbon atom and translating it to a random position. The moves are accepted with a probability

$$P_{\mathrm{acc}} = \min\left[1, \exp\left\{ -\frac{1}{T_\chi}\left[\left(\chi^2_{\mathrm{new}} - \chi^2_{\mathrm{old}}\right) + \frac{1}{T_\psi/T_\chi} \times \left(\psi^2_{\mathrm{new}} - \psi^2_{\mathrm{old}}\right) + \frac{1}{T_\delta/T_\chi}\left(\delta^2_{\mathrm{new}} - \delta^2_{\mathrm{old}}\right)\right]\right\}\right], \quad (4)$$

where the subscripts "old" and "new" indicate the parameters before and after the attempted move, respectively. We assign weightings T_χ, T_δ, and T_ψ to the parameters χ^2, δ^2, and ψ^2, respectively. We then fix the ratios T_ψ/T_χ and T_δ/T_χ to values chosen with a trial-and-error procedure so that satisfactory values of the parameters χ^2, δ^2, and ψ^2 are obtained. T_χ is an effective temperature, which determines the acceptance ratio and is changed during our procedure using simulated annealing [17].

The $g(r)$ of the resulting models for CS400 and CS1000 are shown in Figure 1. We used 5 nm cubic simulation boxes with full periodicity. The peak positions and relative heights of the simulated and target $g(r)$ are in excellent agreement. Snapshots of the resulting structures for CS400 and CS1000 are shown in Figure 2 and Figure 3, respectively. The porosity of CS400 is higher than that of CS1000. Our model shows an increase in the size of graphene segments and stacking of graphene segments with heat treatment temperature. These features are also observed in experimental Transmission Electron Microscopy (TEM) images. Moreover, we developed a methodology to simulate the TEM images of our resulting structural models. The main changes in morphology caused by an increase in heat treatment temperature observed in experimental TEM images, are also present in the simulated TEM images. We have also performed

GCMC simulations of nitrogen at 77 K in these carbons. The adsorption isotherms in both models are significantly different, even though their pore size distributions (the most widely used function to characterize these materials) are very similar. In agreement with experimental studies in nanoporous carbons, the calculated isosteric heat of adsorption in our models decreases with the amount adsorbed. The slit-pore model, however, predicts the opposite trend.

3 Molecular dynamics simulations

We performed micro-canonical molecular dynamics (MD) simulations of a Lennard-Jones fluid confined in the resulting models of CS400 and CS1000 (see Sect. 2) at 77 K and 190 K, and four relative loadings (28%, 46%, 88% and 100%). We modeled the nitrogen-nitrogen and nitrogen-carbon interactions with the Lennard-Jones potential, using the same potential parameters that we used in the grand canonical Monte Carlo (GCMC) simulations of our previous work [6], which are chosen to model nitrogen confined in porous carbons (see Tab. 1).

We used the velocity-Verlet algorithm to integrate the equations of motion (for details, see Ref. [18]), with a time step of 0.009 ps. The initial positions were taken from GCMC simulations of the same fluid at 77 K. The initial velocities were chosen to produce the desired temperatures (77 K and 190 K). We equilibrated the simulations over the first 5000 time steps and collected averages over 65000 time steps, every 10 time steps. We calculated the mean-squared displacement and the velocity autocorrelation function. This calculation was made averaging over all the particles in the system over 4000 time origins. As an example, these functions are shown in Figure 4 for the fluid confined in the CS400 model at 190 K and four loadings.

The velocity autocorrelation function (see Fig. 4a) reaches zero faster as loading increases, indicating that the frequency of collisions increases with loading. The mean-squared displacement (see Fig. 4b) increases rapidly at short times and with a lower slope at larger times. This behavior of the velocity autocorrelation function and mean-squared displacement is observed for both CS400 and CS1000 at the two temperatures studied. For slit pores, it has been found that the mean-squared displacement increases almost linearly in the plane parallel to the pore walls, and increases rapidly at short times and then plateaus at larger times in the direction perpendicular to the pore walls (see [19]). Not surprisingly, the mean-squared displacement in our realistic models seems to be a combination of these two functions. The small values of this function for both structures are due to the fact that many of the pores are closed (see Fig. 2 and Fig. 3), forcing the adsorbate molecules to stay in localized regions of the pore volume. We calculated the self-diffusivities from the mean-squared displacement in the range from 18 to 22 ps using the Einstein relation:

$$D = \frac{1}{6}\frac{\mathrm{d}}{\mathrm{d}t}\left\langle \left|\vec{r}_i(t) - \vec{r}_i(0)\right|^2 \right\rangle, \qquad (5)$$

Table 1. Lennard-Jones potential parameters for nitrogen-nitrogen and nitrogen-carbon interactions [20].

	σ (Å)	ε/k (K)
Nitrogen-nitrogen	3.75	95.2
Nitrogen-carbon	3.36	61.4

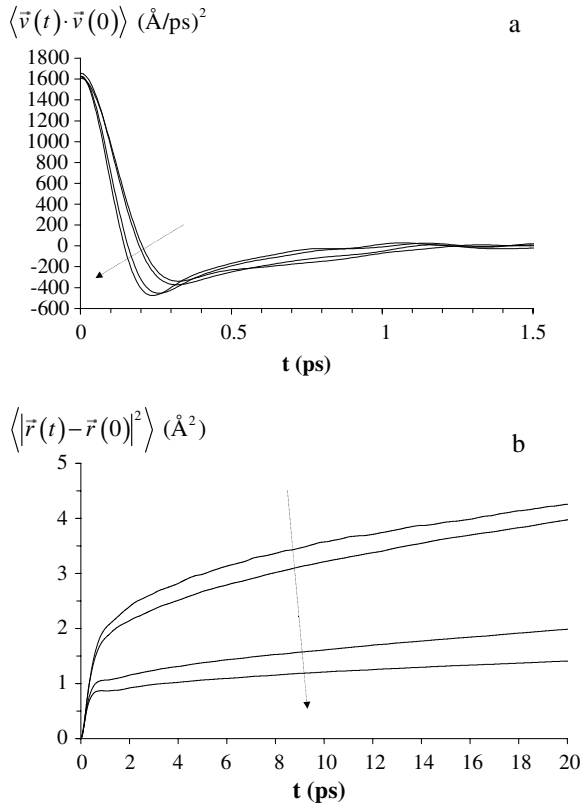

Fig. 4. Velocity auto-correlation function (a) and mean-squared displacement (b) for Lennard-Jones nitrogen confined in the CS400 model at 190 K. Different curves are for different loadings. The loading increases in the direction of the arrow (28%, 46%, 88%, and 100%).

where the expression in the brackets is the mean-squared displacement, calculated as described above. It is important to note that this is an *effective* self-diffusivity, since it is calculated from the slope of the mean-squared displacement in a specific time range. The results are shown in Figure 5.

As expected, the self-diffusivity increases with temperature for both carbon models and for all the loadings studied. The activation energies for diffusion are on the order of 2 kJ/mol. Even though both carbon models have very similar pores size distributions [6], the adsorbate-adsorbent energies are much lower (more attractive) for CS1000 than for CS400 (see Fig. 6) due to differences in the morphology of the two materials. From molecular simulations in slit pores, we know that more attractive energies cause lower self-diffusivities, and this effect is more pronounced at higher adsorbate densities [21]; this may be the reason why, at the same conditions, the self-diffusivity

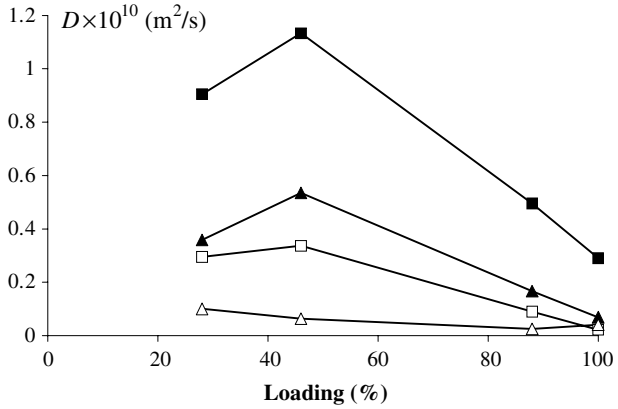

Fig. 5. Self-diffusivity of Lennard-Jones nitrogen confined in the models of CS400 (squares) and CS1000 (triangles) at 77 K (empty symbols) and 190 K (filled symbols).

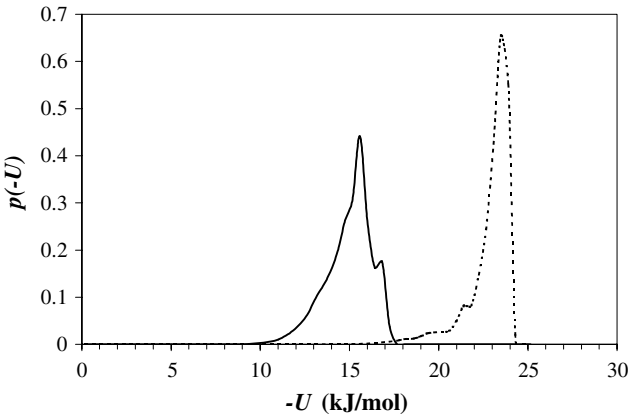

Fig. 6. Adsorbate-adsorbent energy distribution for CS400 (solid line) and CS1000 (broken line). Taken from [6].

is lower in CS1000 than in CS400. Also, the difference in self-diffusivity between CS400 and CS1000 decreases at high loading.

We also observe a maximum in the self-diffusivity as a function of loading in the two carbon models (see Fig. 5). This maximum has not been observed in molecular dynamics simulations of simple fluids confined in slit pores at similar conditions [21,22], where self-diffusivity decreases with loading. However, this behavior has been reported in an experimental study of water in activated carbons [23], and it is also a well-known feature of molecular fluids in zeolites (*e.g.*, [24]). We hypothesize that the maximum is due to the heterogeneity in the adsorbate-adsorbent energy. At lower loadings, the fluid molecules are adsorbed in the sites of lower (more attractive) energies, where they have lower mobility and thus, lower self-diffusivity. As loading increases, the low-energy sites are occupied, and the molecules are adsorbed in sites where they have higher mobility, resulting in a higher self-diffusivity. When loading increases further, the self-diffusivity decreases due to steric hindrance caused by higher adsorbate density.

Self-diffusivities of simple fluids confined in slit pores at similar conditions [19,21] are at least 15 times larger than the ones reported in this work for the same mean pore width. Experimental limiting diffusivities of nitrogen and argon confined in carbon molecular sieves at similar conditions [25], on the other hand, are of the same order of magnitude as the ones reported in this work.

4 Conclusions

We have calculated the effective self-diffusivities of a Lennard-Jones model of nitrogen in two realistic models [6] of saccharose-based carbons heated at 400 °C (CS400) and 1000 °C (CS1000). We carried out molecular dynamics simulations in both models at two temperatures and four loadings. Many of the pores in the resulting models are closed; the adsorbate molecules stay in localized regions of the pore volume. Therefore, the values of the mean-squared displacement for both materials are relatively small, even at times for which the velocity autocorrelation function goes to zero.

We found that self-diffusivity increases with temperature in both carbon models, as expected. Self-diffusivity is lower in CS1000 than in CS400, presumably due to the more attractive adsorbate-adsorbent energies in CS1000. We observe a maximum in self-diffusivity as a function of loading in both models. This behavior has not been observed in molecular dynamics simulations in slit pores, but it has been reported in experimental studies of water in activated carbons [23]. We believe that this behavior is due to the energetic heterogeneity of the carbon. The self-diffusivities reported here are of the same order of magnitude as the diffusivities reported in an experimental study of nitrogen and argon in carbon molecular sieves at similar conditions [25].

We would like to acknowledge the US Department of Energy for funding under DE-FG02-98ER14847, and the National Partnership for Advanced Computer Infrastructure for providing the supercomputer time under the NRAC award MCA93S011.

References

1. T.J. Bandosz, M.J. Biggs, K.E. Gubbins, Y. Hattori, T. Iiyama, K. Kaneko, J. Pikunic, K.T. Thomson, in *Chemistry and Physics of Carbon*, edited by L.R. Radovic (Marcel Dekker, New York) in press.
2. K.T. Thomson, K.E. Gubbins, Langmuir **16**, 5761 (2000).
3. J. Pikunic, R.J.-M. Pellenq, K.T. Thomson, J.-N. Rouzaud, P. Levitz, K.E. Gubbins, Stud. Surf. Sci. Catal. **132**, 647 (2001).
4. J. Pikunic, R.J.-M. Pellenq, K.E. Gubbins, in *Proceedings of Fundamentals of Adsorption 7*, edited by K. Kaneko, H. Kanoh, Y. Hanzawa (IK International, Chiba, 2002) p. 377.
5. J. Pikunic, C. Clinard, N. Cohaut, K.E. Gubbins, J.-M. Guet, R.J.-M. Pellenq, I. Rannou, J.-N. Rouzaud, Stud. Surf. Sci. Catal. **144**, 19 (2002).
6. J. Pikunic, C. Clinard, N. Cohaut, K.E. Gubbins, J.-M. Guet, R.J.-M. Pellenq, I. Rannou, J.-N. Rouzaud, Langmuir **19**, 8565 (2003).

7. A.K. Soper, in *Springer Proceedings in Physics*, edited by M. Davidovic, A.K. Soper, Vol. **40** (Springer-Verlag Berlin, Heidelberg, 1989) p. 189.
8. A.K. Soper, IOP Conf. Proc. **107**, 57 (1990).
9. A. Szczygielska, A. Burian, S. Duber, J.C. Dore, V. Honkimaki, J. Alloys Compounds **328**, 231 (2001).
10. R.L. McGreevy, L. Pusztai, Mol. Simul. **1**, 359 (1988).
11. R. Evans, Mol. Simul. **4**, 409 (1990).
12. R.L. Henderson, Phys. Lett. A **49**, 197 (1974).
13. C.G. Gray, K.E. Gubbins, *Theory of Molecular Fluids* (Clarendon Press, Oxford, 1984) p. 178.
14. D.W. Brenner, Phys. Rev. B **42**, 9458 (1990).
15. J. Tersoff, Phys. Rev. Lett. **61**, 2879 (1988).
16. A.P. Horsfield, A.M. Bratkovsky, M. Fearn, D.G. Pettifor, M. Aoki, Phys. Rev. B **53**, 12694 (1996).
17. S. Kirkpatrick, C.D. Gelatt jr., M.P. Vecchi, Science **220**, 671 (1983).
18. M.P. Allen, D.J. Tildesley, *Computer Simulation of Liquids* (Clarendon Press, Oxford, 1987).
19. S.H. Krishnan, K.G. Ayappa, J. Chem. Phys. **118**, 1 (2003).
20. W.A. Steele, *The Interaction of Gases with Solid Surfaces* (Pergamon Press, Oxford, 1974).
21. S. Suh, D. Nicholson, Mol. Phys. **99**, 383 (2001).
22. R.F. Cracknell, D. Nicholson, K.E. Gubbins, J. Chem. Soc. Faraday Trans. **91**, 1377 (1995).
23. J. Kärger, H. Pfeifer, Pure Appl. Chem. **61**, 1875 (1989).
24. S. Brandani, D.M. Ruthven, J. Karger, Zeolites **15**, 494 (1995).
25. K. Chihara, M. Suzuki, K. Kawazoe, AIChE J. **24**, 237 (1978).